Supporting Information:

Regenerated and Rotation Induced Cellulose-wrapped Oriented CNTs Fibers for Wearable Multifunctional Sensors

Changfei Jing[a], Weihua Liu[b], Huali Hao[c], Huagao Wang[a], Fanbin Meng[a,] *, Denvid Lau[c]

[a] *Department of Materials Science and Engineering, Southwest Jiaotong University, Chengdu 610031, China.*

[b] *Department of Scientific Research, Naval Academy of Aeronautical Engineering, Yantai 264001, China.*

[c] *Department of Architecture and Civil Engineering, City University of Hong Kong, Hong Kong 999077, China.*

E-mail: mengfanbin_wing@126.com (Fanbin Meng)

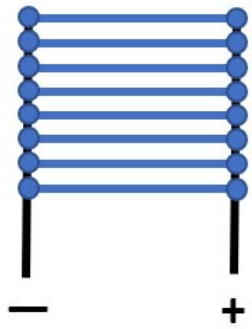

Figure S1. Schematic diagram of coaxial fiber electric heater

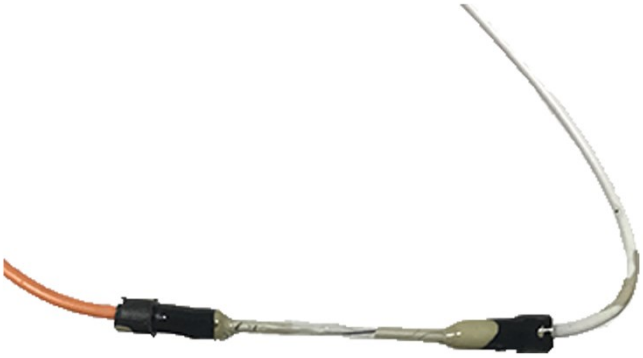

Figure S2. The optical photo of coaxial fiber temperature sensor.

Molecular dynamics (MD) Simulation detail

In our work, the MD simulations have been applied to study how CNTs affect the movements of cellulose chains, figuring out the reason for the performance improvement for CNT/cellulose fiber. There are two parallel chains in the unit cell where one chain (the origin chain) is positioned at the corner of the unit cell parallel to the c axis direction, and the second chain (the center chain) passes through the center of the *ab* plane. Each chain in the unit cell is made up of two glucose residues linked by the β (1–4) glycosidic linkage. The modeled cellulose with a size of 8.0 nm × 8.5 nm × 20 nm is also constructed for comparison.

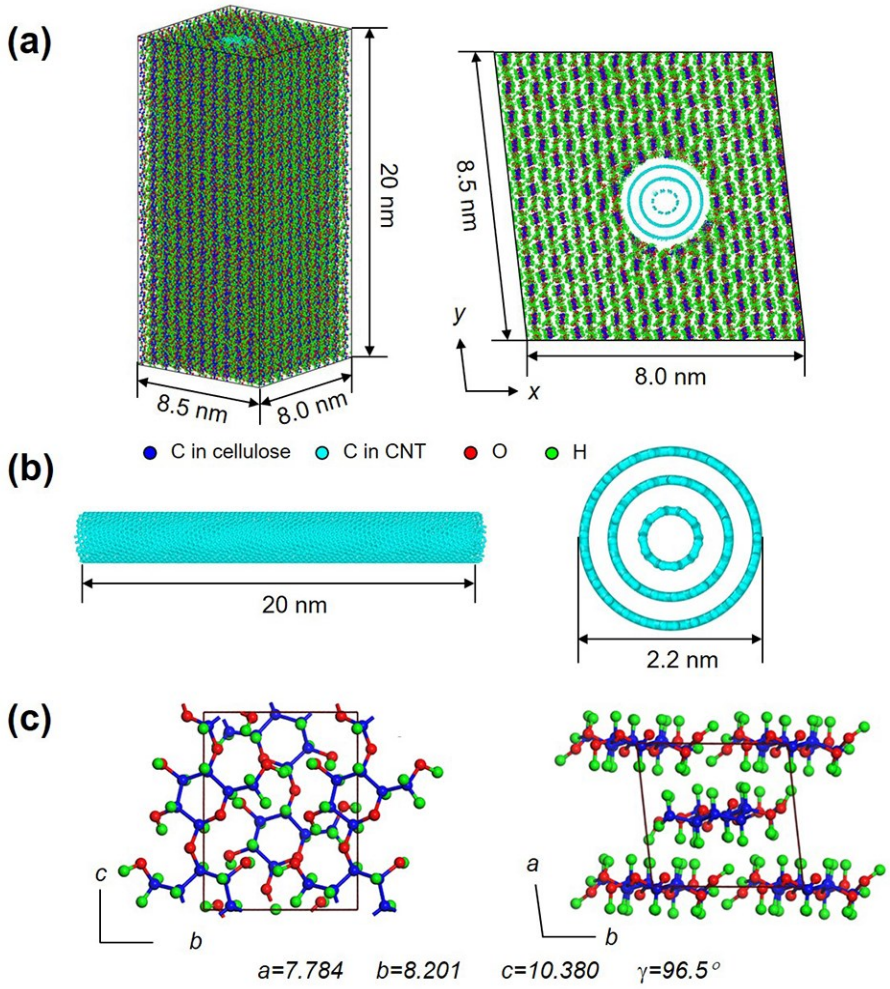

Figure S3. (a) The modeled CNT/cellulose with a size of 7.8 nm × 8.2 nm × 20 nm. (b) The structure of embedded MWCNT with a diameter of 2.2 nm and a length of 20 nm.

(c) The basic monoclinic structure of cellulose fiber. The *x*, *y* and *z* directions are parallel to the [100], [010] and [001] directions of crystalline cellulose respectively.

The intra- and intermolecular interactions in the nanocomposite systems are described by the polymer consistent forcefield (PCFF) [1], which is parametrized from quantum mechanics calculations and works well with polymers and organic materials. The functional form of PCFF is expressed as [1]:

$$\begin{aligned} U = & \sum_{n=2}^{4} K_{b,n}(b - b_0)^4 + \sum_{n=2}^{4} K_{a,n}(\theta - \theta_0)^4 + \sum_{n=1}^{3} K_{t,n}[1 - \cos(n\phi - \phi_n)] + \sum_{out-of-plane} K_{oop}(\chi - \chi_0)^2 \\ & + \sum_{bb'} K_{bb'}(b - b_0)(b' - b_0) + \sum_{ba} K_{ba}(b - b_0)(\theta - \theta_0) + \sum_{aa'} K_{aa}(\theta - \theta_0)(\theta' - \theta_0) + \\ & + \sum_{bt} [K_{bt}(b - b_0) \sum_{n=1}^{3} K_{bt,n} \mathrm{coosn}\phi] + \sum_{at} [K_{at}(\theta - \theta_0) \sum_{n=1}^{3} K_{at,n} \mathrm{coosn}\phi] + \sum_{aat} [K_{aat}(\theta - \theta_0)(\theta' - \theta_0)\cos\phi] \\ & + \sum_{i,j} D_{ij}[2(\frac{r_{ij}}{r})^9 - 3(\frac{r_{ij}}{r})^6] + \sum_{i,j} C \frac{q_i q_j}{\varepsilon r_{ij}} \end{aligned} \quad \text{(S1)}$$

The potential energy comprises a set of covalent related interactions such as the bond interaction between pairs of bonded atoms, the angle interaction between three consecutive bonded atoms, the dihedral and the improper interaction between quadruplets of atoms, the cross-terms such as bond-bond, bond-angle, angle-angle, bond-torsion, angle-torsion, and angle-angle-torsion coupling terms and non-bonded interactions like van der Waals interaction and the Coulombic interaction. The predicted physicomechanical and thermal properties of cellulose had been found in good agreement with experimental data [2]. The properties of CNT [3] and the interfacial interactions between CNT and polymers such as graphene and epoxy [4, 5] can be characterized by PCFF, which is well correlated to experimental findings. All these indicate the reliability of PCFF to predict the properties of CNT/cellulose.

All MD simulations are carried out using the parallel MD code LAMMPS [6]. A periodic boundary condition is applied to three directions of the modeled CNT/cellulose and cellulose systems. The initial configurations are first equilibrated in the isothermal and isochoric (NVT) ensemble at the temperature of 300 K for 1 ns followed by another 5 ns equilibrated in the isothermal and isobaric (NPT) ensemble at 300 K and 1 atm. The root-mean-square displacement (RMSD) of the atoms reaches a constant level before the competition of equilibration, which indicates that the systems have been appropriately equilibrated. The tensile deformation of the equilibrated systems is performed by applying a fixed strain rate of 10^{-4}/ps to the length direction at 300 K.

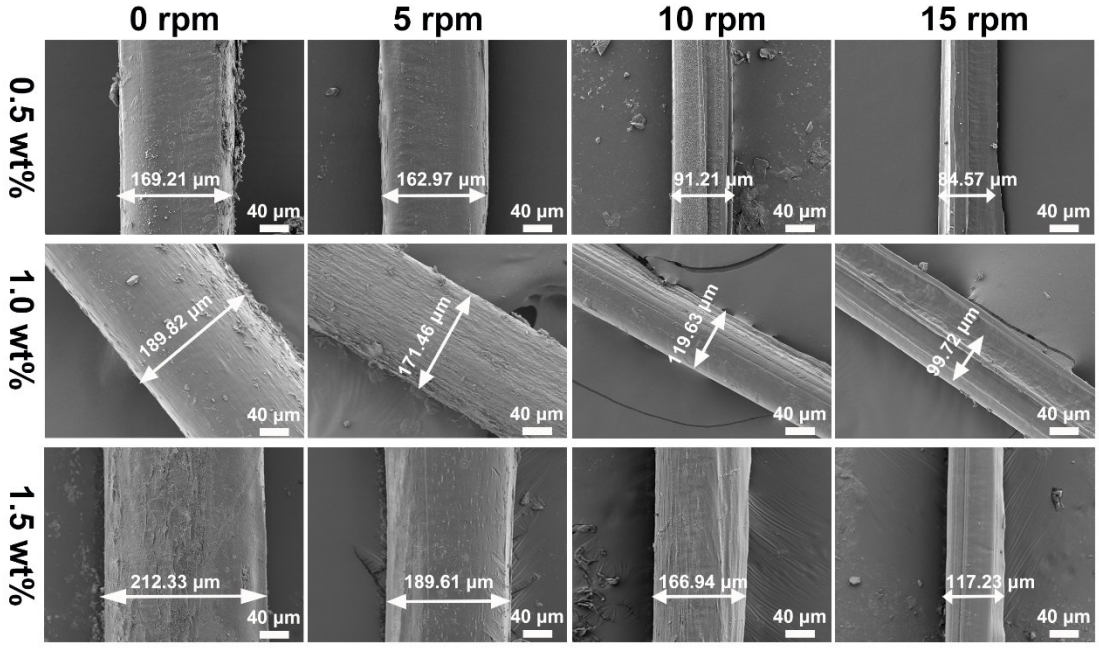

Figure S4. SEM images of the composite fibers under different addition content of CNTs and rotational speeds. Each row represents coaxial fibers with different MWCNTs concentrations. Each column represents coaxial fibers with different rotating speeds.

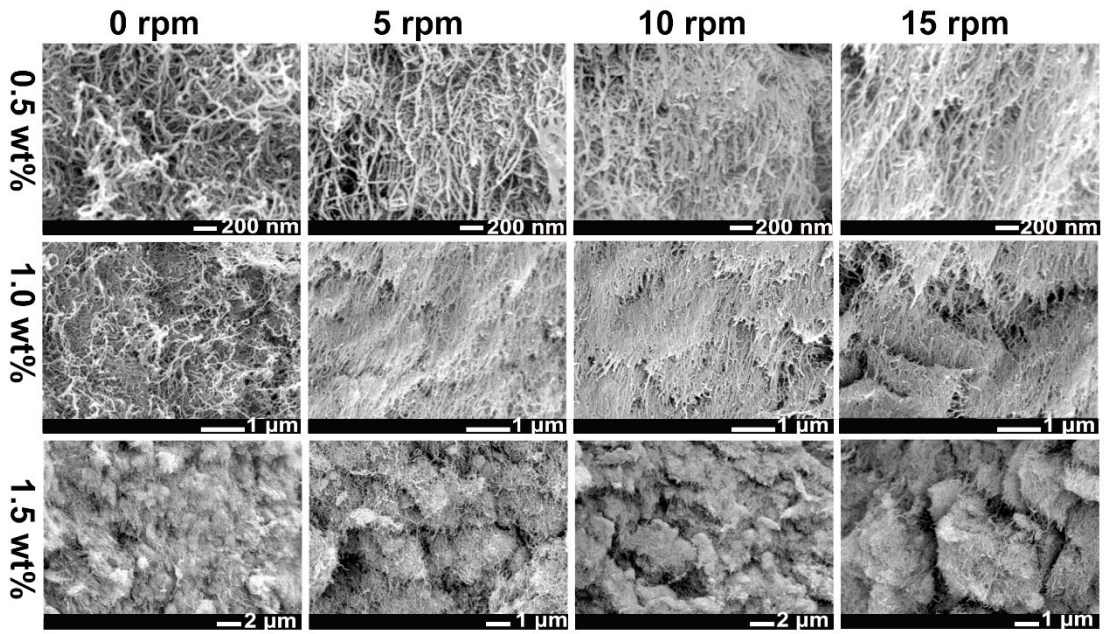

Figure S5. The cross-sectional SEM image of the composite fibers under different addition content of CNTs and rotational speeds. Each row represents composite fibers with different CNTs contents. Each column represents composite fibers with different rotational speeds.

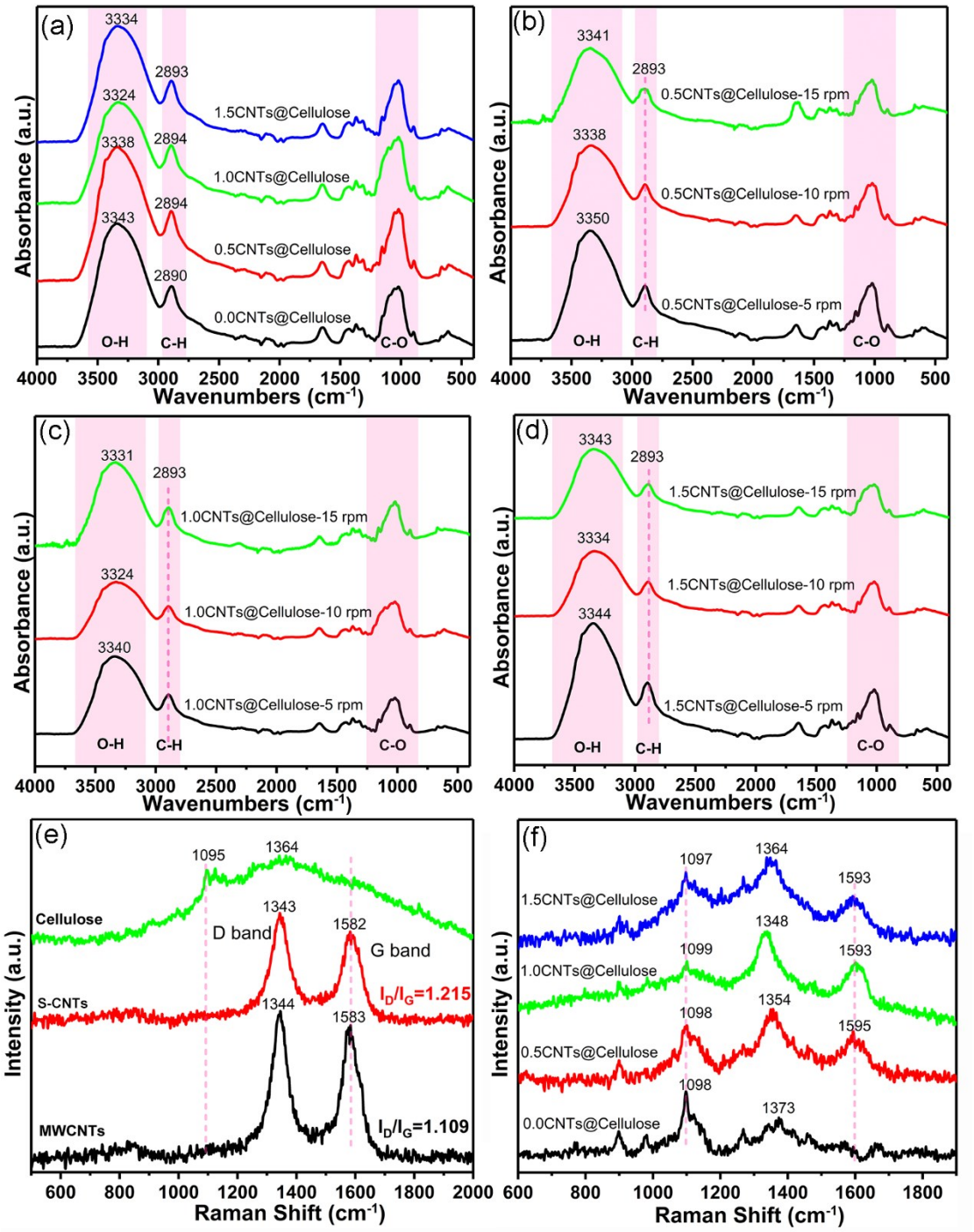

Figure S6. The structure characteristics of the composite fibers. (a) FTIR spectra of xCNTs@Cellulose-10rpm composite fibers. (b-d) FTIR spectra of the composite fibers at different rotational speeds with CNTs content of 0.5 wt%, 1 wt% and 1.5 wt%, respectively. (e) Raman spectroscopy of microcrystalline cellulose (Cellulose), multi-walled carbon nanotubes (MWCNTs) and CNTs dispersed by sulfuric acid (S-CNTs). (f) Raman Spectroscopy of composite fibers at 10rpm and different CNTs contents.

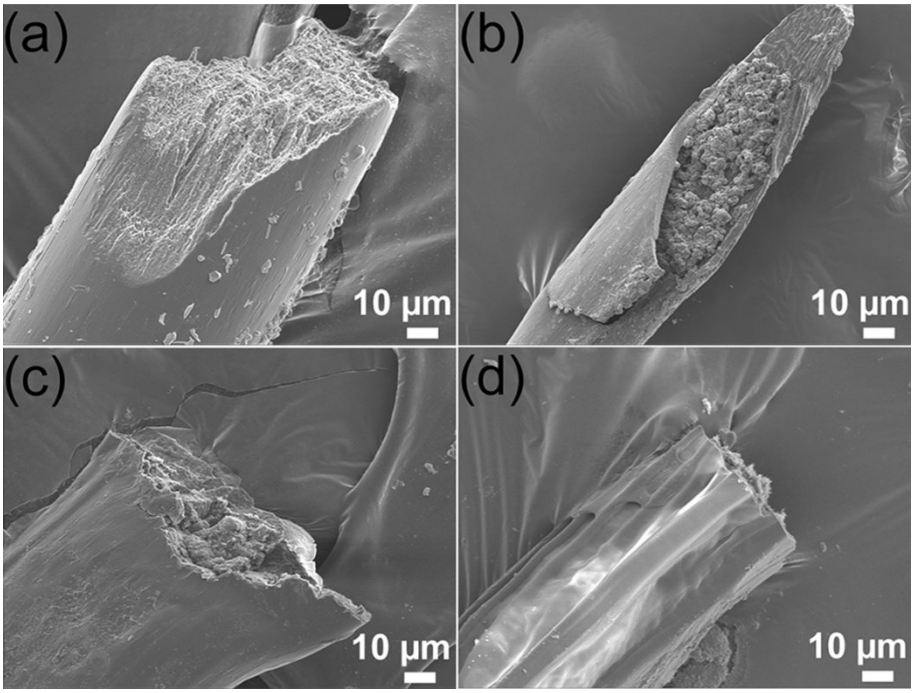

Figure S7. The SEM images of the end of fibers with different CNTs contents. (a-d) The content of CNTs is 0 wt%, 0.5 wt%, 1.0 wt% and 1.5 wt%, respectively.

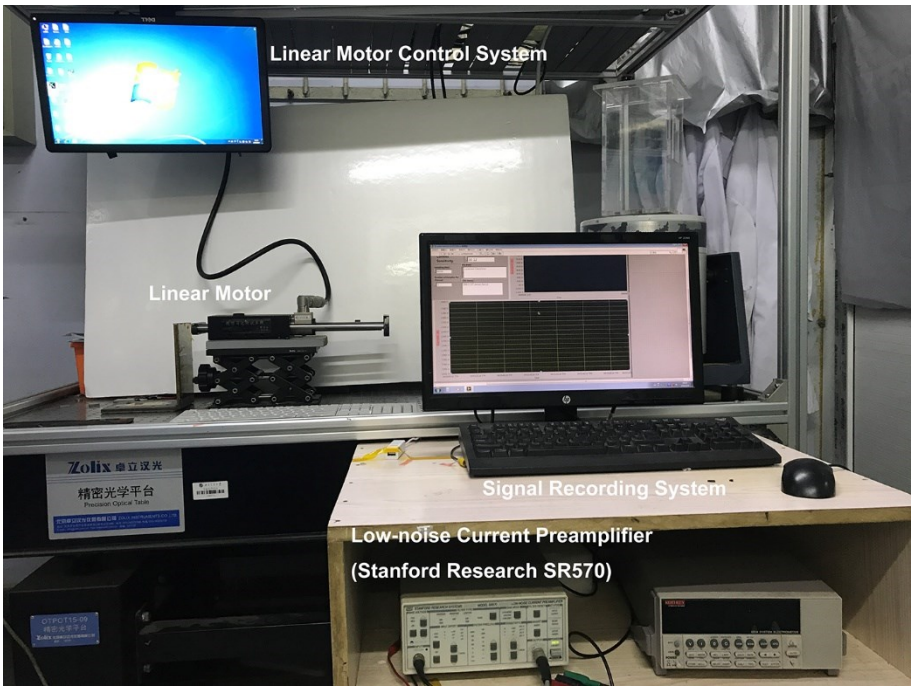

Figure S8. Self-made strain sensing monitoring system.

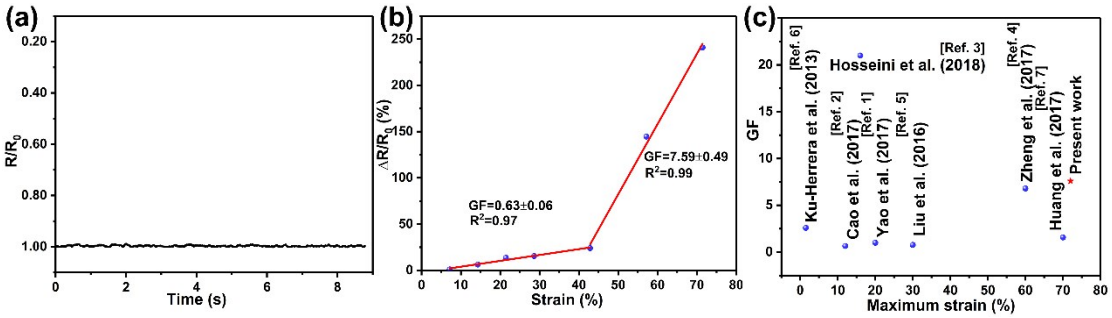

Figure S9. The Strain sensing performance of CNTs@Cellulose fibers. a) The resistance of the blank control group without the carbon tube changed, when the strain was applied. (b) The GF factor of Coaxial Fibers. The GF factor of coaxial fibers was obtained by fitting the strain test data. (c) A comparison with the recently reported work on cellulose [7-13].

$$GF=\frac{\Delta R/R_0}{\varepsilon} \quad (S2)$$

In the above formula, R_0 represents the initial resistance, $\Delta R/R_0$ is the relative change in resistance, and ε is the applied strain. Therefore, the GF factor can be obtained by fitting the slope of the curve [14-17].

The temperature sensor execution code is as follows:

```
#include <Wire.h>
#include <LiquidCrystal_I2C.h>
LiquidCrystal_I2C lcd(0x27,16,2);
int potPin = A0;
float temperature = 0;
float val=0;
void setup() {
lcd.init();
delay(20);
lcd.init();
delay(20);
lcd.backlight();
Serial.begin(9600); }
void loop()
{
   val=analogRead(potPin);
   temperature = (-5.88235*val+3142.46471);// Determined based on the
electrochemical properties of the MWCNTs@Cellulose fibers.
lcd.clear();
lcd.setCursor(0, 0);
```

```
{
lcd.print("Temperature");
}
lcd.setCursor(7, 1);
{
lcd.print(temperature);
  Serial.println(val,3);
lcd.write (0xdf);
lcd.write (0x43);
}
delay(500);
}
```

REFERENCES

1. H. Sun, S. J. Mumby, J. R. Maple and A. T. Hagler, *J. Am. Chem. Soc.*, 1994, **116**, 2978-2987.
2. W. Wang, Y. Wang and X. Li, *BioResources*, 2018, **13**, 7900-7910.
3. J. Lee, V. Varshney, A. K. Roy and B. L. Farmer, *The Journal of chemical physics*, 2011, **135**, 104109.
4. R. Rahman, J. T. Foster and A. Haque, *The Journal of Physical Chemistry A*, 2013, **117**, 5344-5353.
5. W. Jian and D. Lau, *Carbon*, 2019, **153**, 745-756.
6. S. Plimpton, *J. Comput. Phys.*, 1995, **117**, 1-19.
7. H. Hosseini, M. Kokabi and S. M. Mousavi, *Carbohydr. Polym.*, 2018, **201**, 228-235.
8. X. Cao, X. Wei, G. Li, C. Hu, K. Dai, J. Guo, G. Zheng, C. Liu, C. Shen and Z. Guo, *Polymer*, 2017, **112**, 1-9.
9. Y. Zheng, Y. Li, K. Dai, M. Liu, K. Zhou, G. Zheng, C. Liu and C. Shen, *Compos. Part A-Appl. S.*, 2017, **101**, 41-49.
10. H. Liu, Y. Li, K. Dai, G. Zheng, C. Liu, C. Shen, X. Yan, J. Guo and Z. Guo, *J. Mter. Chem. C*, 2016, **4**, 157-166.
11. Z. M. Huang, X. Y. Liu, W. G. Wu, Y. Q. Li and H. Wang, *J. Mater. Sci.*, 2017, **52**, 12540-12552.
12. Q. Yao, B. Fan, Y. Xiong, C. Wang, H. Wang, C. Jin and Q. Sun, *Carbohydr. Polym.*, 2017, **168**, 265-273.
13. J. K. Herrera, F. Avilés and G. Seidel, *Smart Mater. Struct.*, 2013, **22**, 085003.
14. J. Zhou, X. Xu, Y. Xin and G. Lubineau, *Adv. Funct. Mater.*, 2018, **28**, 1705591.
15. S. Chen, Y. Song, D. Ding, Z. Ling and F. Xu, *Adv. Funct. Mater.*, 2018, **28**, 1802547.
16. Z. Ma, S. Kang, J. Ma, L. Shao, A. Wei, C. Liang, J. Gu, B. Yang, D. Dong and L. Wei, *ACS Nano*, 2019, **13**, 7578-7590.
17. H. Wu, Q. Liu, H. Chen, G. Shi and C. Li, *Nanoscale*, 2018, **10**, 17512-17519.

Video S1 Fiber preparation process in the side view direction

Video S2 Fiber preparation process in a top view

Video S3 The relative resistance change varies periodically in the sensing of bending of the finger

Video S4 The electrothermal properties of CNTs@Cellulose fibers at applied voltage of 5V and 10V.

Video S5 Temperature sensing performance of 1.0CNTs@Cellulose-10rpm fibers.